Dalton Transactions

Conformational Dynamicity in a Copper(II) Coordination Complex

Journal:	*Dalton Transactions*
Manuscript ID	DT-ART-04-2023-001213.R1
Article Type:	Paper
Date Submitted by the Author:	26-May-2023
Complete List of Authors:	Griffin, Paul; University of Illinois Urbana-Champaign, Chemistry Dake, Matthew; University of Illinois Urbana-Champaign, Chemistry Remolina, Alesandro; University of Illinois Urbana-Champaign, Chemistry Olshansky, Lisa; University of Illinois at Urbana-Champaign, Chemistry

ARTICLE

Conformational Dynamicity in a Copper(II) Coordination Complex

Paul J. Griffin, Matthew J. Dake, Alesandro D. Remolina, and Lisa Olshansky*

Received 00th January 20xx,
Accepted 00th January 20xx

DOI: 10.1039/x0xx00000x

The geometries of copper coordination complexes are intricately related to their electron transfer capabilities, but the role of dynamics in these processes are not fully understood. We have previously reported CuCl(dpa^{OMe}), a complex exhibiting conformational fluxionality in its Cu^{I} state and rigidity upon oxidation to Cu^{II}. Here, we report the synthesis and characterization of [CuCl(dpa^{SMe})]$^{+/0}$, a complex exhibiting relative rigidity in its Cu^{I} state and structural dynamics upon oxidation to Cu^{II}. The dynamics of [CuCl(dpa^{SMe})]$^{+}$ were characterized via X-ray diffraction, cyclic voltammetry, and EPR spectroscopy, where temperature-dependent interconversion between trigonal bipyramidal and square pyramidal geometries is observed. Coupling these solid and solution-state characterization data enabled assignment of the coordination geometries involved. Factors impacting these dynamics and their potential implications for electron transfer are discussed.

Introduction

The reactivity and electron transfer capabilities of copper complexes are directly related to the coordination geometry adopted by these compounds.[1] Cu^{I} is a d^{10} metal ion whose coordination complexes have no ligand field stabilization, tending to adopt linear, trigonal planar, or tetrahedral geometries. Cu^{II} is a d^{9} metal ion which undergoes Jahn-Teller distortion, resulting in the predominance of tetragonal and trigonal bipyramidal coordination geometries.[2] Blue copper proteins leverage these differential coordination properties to facilitate rapid electron transfer.[3,4] By holding their copper ion in a coordination geometry that is intermediate between those preferred by either oxidation state, an "entatic state" is formed and rapid electron transfer is achieved.[3–8] In molecular systems, we generally lack the control that the protein framework has to enforce such entatic states. An alternative approach is to design fluxional coordination complexes that give rise to transient entatic states.[9]

We have previously reported conformationally dynamic Cu^{I} complexes containing a dpa^{OMe} (dipicolylaminoaniline) ligand which rigidifies to a square pyramidal coordination geometry upon oxidation.[10] In accordance with "hard-soft acid-base" theory,[11] the dpa^{OMe} ligand was designed with a 'hard' -OMe substituent to bind only in the Cu^{II} oxidation state.[9,10] Herein, we invert this paradigm by installing a 'soft' sulfur donor in place of the oxygen donor present in dpa^{OMe} to create dpa^{SMe}. Solid-state and solution-phase characterization of these complexes reveal that [CuCl(dpa^{SMe})]PF_6 exhibits multiple discrete coordination geometries in its Cu^{II} oxidation state. Powder EPR and single crystal X-ray diffraction (XRD) support assignment of these structures as trigonal bipyramidal and square pyramidal in the solid-state. Solution-phase EPR spectroscopy at variable temperatures demonstrate interconversion from the trigonal bipyramid to the square pyramid as the temperature decreases, a result corroborated by DFT calculations. The electrochemical reversibility of the Cu$^{II/I}$ redox couple is also presented. Ultimately, the interplay between coordination dynamicity and electron transfer capabilities represents a key heuristic for designing redox mediators with first row transition metals.

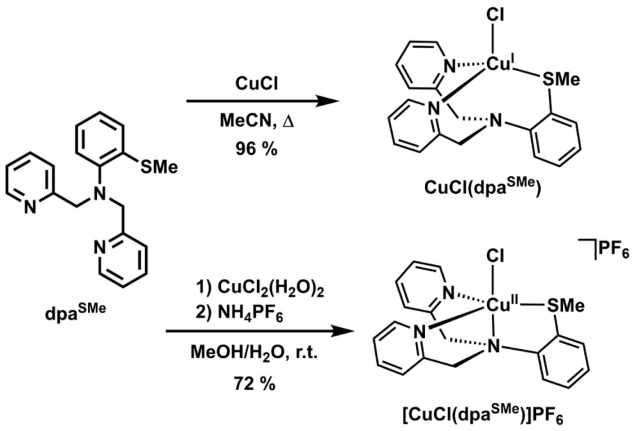

Scheme 1. Synthesis of the [CuCl(dpa^{SMe})]$^{+/0}$ complexes under study. Our previously reported [CuCl(dpa^{OMe})]$^{+/0}$ complexes featured O instead of S in the dpa^{XMe} ligand.

Results

Synthesis of Copper Complexes

The new complexes with dpa^{SMe} were synthesized according to Scheme 1 and characterized by standard spectroscopic methods. High-resolution mass spectrometry, elemental analysis, and single

[a] *Department of Chemistry, Center for Biophysics and Quantitative Biology, and Materials Research Laboratory, University of Illinois at Urbana-Champaign, Urbana, Illinois, 618081, United States.*

Electronic Supplementary Information (ESI) available: ^{1}H- and ^{13}C-NMR spectra, electronic absorption spectra, EPR spectra and simulations, further electrochemical characterization, DFT-optimized coordinates, and crystallographic data (PDF). CCDC 2258225, 2258226, 2258227. See DOI: 10.1039/x0xx00000x

Table 1. Select Bond Lengths (Å), Angles (°), and Distortion Parameters for Complexes Under Study.

	$CuCl(dpa^{SMe})$	$[CuCl(dpa^{SMe})]PF_6$	$[CuCl(dpa^{SMe})]PF_6$
Cu–N_1	2.0880(9)	2.089(2)	1.990(3)
Cu–N_2	2.624[c]	2.070(2)	2.095(3)
Cu–N_3	2.0404(9)	2.016(2)	2.000(3)
Cu–S	2.3493(3)	2.4013(6)	2.5917(9)
Cu–Cl	2.3128(3)	2.2241(6)	2.2820(8)
Cl–Cu–N1	107.49(3)	98.08(7)	97.03(9)
Cl–Cu–N2	177.64	179.40(6)	176.98(7)
Cl–Cu–N3	108.27(3)	98.15(7)	97.42(8)
Cl–Cu–S	108.02(1)	94.27(3)	98.24(4)
S–Cu–N1	100.60(3)	102.86(7)	94.89(8)
S–Cu–N2	69.87	85.40(6)	84.77(7)
S–Cu–N3	113.68(3)	129.04(7)	89.14(8)
N1–Cu–N2	72.18	81.50(9)	87.9(1)
N1–Cu–N3	118.17(4)	123.68(9)	164.3(1)
N2–Cu–N3	73.77	82.45(9)	82.4(1)
τ	0.84[a]	0.84[b]	0.21[b]
Geometry	Tetrahedral	Trigonal bipyramidal	Square pyramidal

[a]τ_4 calculated according to ref 12. [b]τ_5 calculated according to ref 15, where $\tau_5 = 0$ corresponds to ideal square pyramidal and $\tau_5 = 1$ to trigonal bipyramidal coordination geometries. [c]Not a bond

crystal XRD of these compounds are consistent with their assignment as mononuclear complexes. The yield of $CuCl(dpa^{SMe})$ is strongly dependent on the purity of the CuCl precursor – any yellow, tan, or pale-green discoloration of the salt leads to marked decreases in the isolated yield when compared to freshly purified gray/white CuCl (9 % vs 96 %).

The colour of the isolated Cu^{II} complex, $[CuCl(dpa^{SMe})]PF_6$, changes reversibly from green to blue when exposed to air and vacuum, respectively. However, UV-vis absorption spectra of both solids (Figure S1) suggests the powders adopt identical geometries in solution. Moreover, the spectral signature of the *d* → *d* transition does not change significantly when the solvent is changed across a wide range of polarities (Table S1). These different colorations signify different coordination geometries in the solid state and reflect the ability of these complexes to freely interconvert between stereoisomers under ambient conditions.

Structural Characterization by X-Ray Diffraction (XRD)

Single crystals of $CuCl(dpa^{SMe})$ and $[CuCl(dpa^{SMe})]PF_6$ were grown via vapour diffusion of pentane into DCM at room temperature and –20 °C, respectively (for data/refinement parameters, see Tables S2–S4). Both complexes crystallize as monomers in the solid state and exhibit the bond lengths and angles compiled in Table 1.

As shown in Figure 1a, $CuCl(dpa^{SMe})$ crystallizes in a distorted tetrahedral coordination geometry with $\tau_4 = 0.23$.[12] The primary coordination sphere consists of Cl, two N_{pyr} atoms (N1 and N3), and an aryl thioether. The Cu–N_{pyr} bond lengths of 2.0880(9) and 2.0404(9) Å are fairly standard among $CuCl(dpa^{R})$ complexes, while the Cu–Cl bond is slightly lengthened by ~0.06 Å to 2.3128(3) Å compared to analogues in which R = OMe.[9,10,13] The ligand field is completed by a strong Cu–S bond of 2.3493(3) Å. $[Cu(dpa^{SMe})][B(C_6F_5)_4]$, a related Cu^{I} complex reported by Karlin et al.,[14] lacks an inner sphere chloride ligand and instead has its fourth coordination site occupied by the aniline nitrogen (N2) of dpa^{SMe}. This complex has a Cu–N distance of 2.181(2) Å.[14] In contrast, the Cu–N2 distance of 2.6241(9) Å in $CuCl(dpa^{SMe})$ is greater than the sum of the van der Waals radii of copper and nitrogen. The lack of a Cu–N2 bond places Cu^{I} in a pseudo-tetrahedral coordination geometry. Notably, in our previous reports on Cu^{I} complexes with the dpa^{OMe} framework, the methoxy-substituents do not bind to Cu^{I}. Instead the fourth site is occupied by N2.[9,10]

Layer diffusion of methanolic solutions of $[CuCl(dpa^{SMe})]PF_6$ into water affords a mixture of blue and green crystals. XRD structure solutions support that these crystals correspond to trigonal bipyramidal (Figure 1b) and square pyramidal (Figure 1c) coordination geometries, respectively. The trigonal bipyramidal complex ($\tau_5 = 0.84$) [15] has an equatorial plane defined by the pyridine nitrogen atoms (N1 an N3) and the thioether, while N2 and Cl occupy apical positions. The Cu–N_{pyr} distances of 2.089(2) and 2.016(2) Å are approximately the same as in $CuCl(dpa^{SMe})$ with a slight lengthening of the Cu–S bond to 2.4013(6) Å. The apical aniline nitrogen N2 is bound at a distance of 2.070(2) while the Cu–Cl bond contracts to 2.2241(6) Å. Trigonal bipyramidal coordination geometries are common to Cu complexes containing tris(2-pyridylmethyl)amine (tpa) ligands.[16,17]

The isomeric square pyramidal crystal structure ($\tau_5 = 0.21$) is provided in Figure 1c. Karlin et al. report an analogous $[Cu(MeOH)(dpa^{SMe})][ClO_4]_2$ complex that is square pyramidal with no trigonal bipyramidal conformers observed.[14] Similarly, our previously reported structures of $[CuCl(dpaa^{OMe})]BPh_4$[9] and $[CuCl(dpa^{OMe})]PF_6$[10] exclusively crystallize as square pyramidal complexes. The only significant difference here is that the structure of square pyramidal $[CuCl(dpa^{SMe})]PF_6$ is slightly more distorted from the ideal geometry and has a Cu–S bond distance of 2.5917(9) Å, lengthened by ~0.30 Å

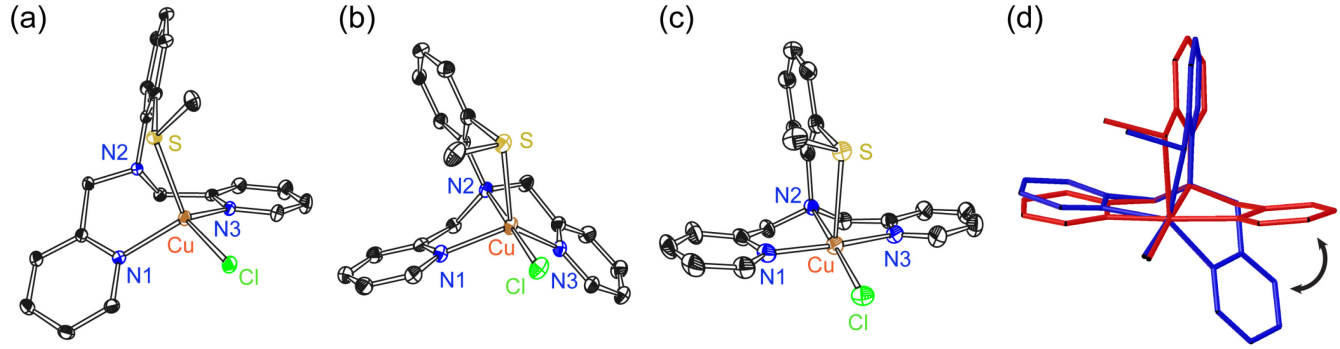

Figure 1. Solid-state structures of CuCl(dpa^{SMe}) (a), trigonal bipyramidal [CuCl(dpa^{SMe})]PF_6 (b), square pyramidal [CuCl(dpa^{SMe})]PF_6 (c), and an overlay of the trigonal bipyramidal (blue) and square pyramidal (red) coordination geometries observed for [CuCl(dpa^{SMe})]PF_6 (d) with thermal ellipsoids at 50 % plotted in ORTEP. H-atoms, solvent molecules, and counterions omitted for clarity.

relative to its dpa^{OMe} congeners. This Cu–S bond is also ~0.06 Å longer than in [Cu(MeOH)(dpa^{SMe})][ClO_4]$_2$, which is believed to retain a square pyramidal geometry in solution.[14,18] The axial Cu–S bond of square pyramidal [CuCl(dpa^{SMe})]PF_6 is also ~0.2 Å longer than the equatorial Cu–S distance observed in the trigonal bipyramidal isomer. These differences are consistent with established structural trends in Cu^{II} complexes.[19]

The dark blue crystals of the square pyramidal species slowly turn green when exposed to solvents they are insoluble in (25% DCM:toluene, EtOH, paratone oil, etc.) with visible cracking of the crystals observed as the structure changes. This green colour matches the observed colour of the freshly prepared trigonal bipyramidal crystals, which may be obtained by layering EtOH or 25% DCM/toluene over the blue crystals. The colour change suggests an interchange between the two geometries. An overlay of the two structures is shown in Figure 1d and reveals that this coordination geometry change may be achieved with minimal perturbation via rotation of one picolyl arm of the ligand. The corresponding N1–Cu–N3 bond angle contracts from 164.3(1)° to 123.68(9)° when converting between the square pyramidal and trigonal bipyramidal geometries. A concomitant expansion of the S–Cu–N3 angle from 89.14(8)° to 129.04(7)° is also observed as the sulfur atom switches between axial and equatorial coordination modes in the square pyramidal and trigonal bipyramidal structures, respectively. The other bond angles in this complex remain relatively unchanged, reflecting the small structural distortions required for this exchange. The geometries of these solids in the bulk – square pyramidal for the blue compound and trigonal bipyramidal for the green powder – were verified by solid-state EPR spectroscopy (*vide infra*).

Nuclear Magnetic Resonance Spectroscopy (NMR)

The ^{1}H-NMR spectrum of CuCl(dpa^{SMe}) was collected in CD_2Cl_2 to confirm the ligand had bound CuCl and to determine if the conformational fluxionality typically observed in CuCl(dpa^R) (R = H, OMe)[10] systems was taking place. The ^{1}H-NMR spectrum of CuCl(dpa^{SMe}) at room temperature exhibits relatively sharp features consistent with a minimally dynamic Cu^I framework in solution. Deshielding of the pyridine resonances by ~0.2 ppm suggests ligation of Cu^I through the pyridines in solution as in other CuCl(dpa^R).[9,10] However, in contrast to CuCl(dpa^{OMe}), where shielding of the -OMe resonance is observed, here we observe deshielding of the -SMe protons by 0.12 ppm (Figure S2). This deshielding suggests that a Cu–S bond exists in solution,[20] and that the crystallographically observed coordination at Cu^I is maintained in solutions with noncoordinating solvents such as DCM.

Electron Paramagnetic Resonance Spectroscopy (EPR)

Our ability to isolate [CuCl(dpa^{SMe})]PF_6 as two interchangeably coloured powders, blue and green, that resembled the solids used in XRD experiments, facilitated characterization of the geometries for the bulk samples discretely via solid-state EPR spectroscopy. Solid-state EPR spectra of blue (Figure S3a) and green (Figure S3b) [CuCl(dpa^{SMe})]PF_6 were collected at room temperature as the powders in finely ground 50 % v/v mixtures with [Bu_4N]PF_6. A control spectrum of pure [Bu_4N]PF_6 revealed no paramagnetic impurities within the experimental range, supporting that the subsequent absorption features arise from the Cu^{II} complexes themselves. The spectrum of the blue powder could be modelled as a single species in an axial coordination environment ($g_\perp$ = 2.06, $g_{||}$ = 2.17), consistent with the square pyramidal geometry observed crystallographically for the blue crystals. The green powder was simulated as a single rhombic species that is consistent with the trigonal bipyramidal geometry (g_1 = 2.02, g_2 = 2.12, g_3 = 2.22)

Table 2. EPR Simulation Parameters for Cu^{II} Complex in Different Geometries.

	g_1	g_2	g_3	$A_{\|}$ (MHz)	g_{iso}	A_{iso} (MHz)
Powder[a]						
Blue solid	2.06	2.17	2.17	---	---	---
Green solid	2.02	2.12	2.22	---	---	---
Solution[b]						
77K	2.06	2.25	2.25	500	---	---
298K	---	---	---	---	2.01	158
DFT[c]						
Trigonal bipyramidal	2.01	2.11	2.16		2.094	140
Square pyramidal	2.04	2.05	2.16		2.087	253

[a]50 % v/v mixture with [NBu_4]PF_6. [b]3.6 mM Cu^{II} in 1:1 DMF : toluene. [c]Calculated at B3LYP level of theory with def-TZVPP basis on non-H atoms.

observed crystallographically for the green crystals. Neither species exhibits observable hyperfine coupling to the I = 3/2 nucleus of Cu in the solid-state (for X-band measurements conducted at room temperature.) DFT calculations for the complex in both geometries afford g-values in good agreement with experimental data (Table 2).

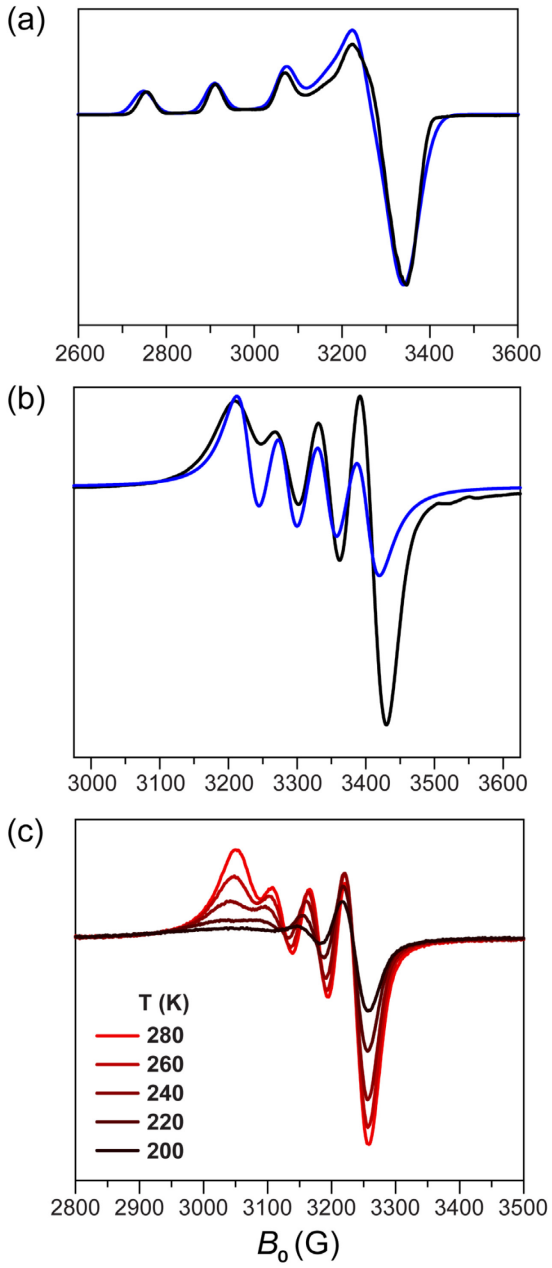

Figure 2. EPR spectra (black) and simulations (blue) of 3.6 mM solutions of [CuCl(dpa^{SMe})]PF_6 in 1:1 DMF : toluene collected at 77 K (a), and 298 K (b). Variable-temperature measurements in solutions of 1:1 DCM:toluene collected at the indicated temperatures (c).

Initial work to probe the solution-phase coordination geometry by EPR spectroscopy was performed in 1:1 toluene/DMF solutions, which glass at 77 K. As shown in Figure 2a, the Cu^{II} complex exhibits the expected hyperfine splitting pattern for an I = 3/2 nucleus of naturally abundant Cu along $g_{||}$, which was reasonably simulated with a single axial species ($g_{\perp}$ = 2.06, $g_{||}$ = 2.25, and A_{Cu} = 64 and 500 MHz, respectively), suggesting a square pyramidal coordination geometry in solution at 77 K (Table 2). The spectrum of this isomer resembles those previously reported for [CuCl(dpa^{OMe})]PF_6 under similar conditions, suggesting that the identity of -SMe vs -OMe as an axial ligand does not strongly impact the electronic structure of the tetragonal isomer of the Cu^{II} complex.[10]

Reasoning that the trigonal bipyramidal isomer – which was not observed in the 77 K glass – might be observable at other temperatures, the solution-phase EPR spectrum was collected at 298 K. As shown in Figure 2b, the solution-phase EPR spectrum at room temperature is best simulated as an isotropic spectrum of a single species with g_{iso} = 2.01 and A_{iso} = 153 MHz (Table 2). These isotropic parameters closely correspond to those calculated for a trigonal bipyramidal species in solution (g_{iso} = 2.094, A_{iso} = 140 MHz) and disagree with those calculated for a square pyramid (g_{iso} = 2.087, A_{iso} = 253 MHz), leading us to assign the solution-phase structure of the species at room temperature as a trigonal bipyramid. Of note is that the major difference between the isomers manifests in the extent of hyperfine coupling rather than significant changes in g (Figure S4).

To explore a wider temperature window for variable-temperature experiments, EPR spectra were collected on samples in 1:1 DCM/toluene mixtures. Solution phase EPR spectra of [CuCl(dpa^{SMe})]PF_6 at 280 K in 1:1 DCM/toluene are to those collected in 1:1 DMF/toluene described above (g_{iso} = 2.12 and A_{iso} = 158 MHz, Figure S5). The good agreement between these two solvent conditions is corroborated by steady-state UV-vis absorption measurements in which the $d \rightarrow d$ transitions observed mimic those in other trigonal bipyramidal complexes (Figure S1, Table S1).[21,22] This agreement suggests that the trigonal bipyramidal structure, and corresponding conformational equilibrium is conserved in both solvents. Variable-temperature EPR spectroscopy was performed over the range 280–200 K and reveals qualitative changes as the temperature decreases (Figure 2c). Modelling to a single isotropic species also becomes increasingly difficult as the temperature decreases, particularly below 240 K. Below this temperature, the analyte may cross from the isotropic regime into the regime in which anisotropic contributions are introduced.[23] This so-called 'slow motion regime' becomes important as DCM approaches its freezing point (176.5 K) and the viscosity of the medium increases. Though challenging to fit, these lower temperature spectra begin to qualitatively resemble the EPR spectrum observed in the 77 K glass (Figure 2a). Our interpretation of these data is that the solution-phase geometry approximates square pyramidal as the temperature decreases, while the trigonal bipyramidal geometry predominates at room temperature. No such dynamicity is observed in the case of [CuCl(dpa^{OMe})]PF_6.

Electrochemistry

Cyclic voltammograms (CVs) of [CuCl(dpa^{SMe})]PF_6 collected in DCM with scan rates ranging from 25 to 500 mV/s are shown in Figure 3, with parameters listed in Table S5. A plot of current density vs the square root of the scan rate indicates that the $Cu^{II/I}$ couple is under diffusion control and not adsorbed on the electrode surface (Figure S6). A single reversible redox event is observed at –430 mV vs $Fc^{+/0}$, with $i_a/i_c \approx 1$, and $E_a–E_c$ = 110 mV ($E_a–E_c$ = 140 mV for $Fc^{+/0}$). The reversibility of the $Cu^{II/I}$ event is unusual in the context of copper

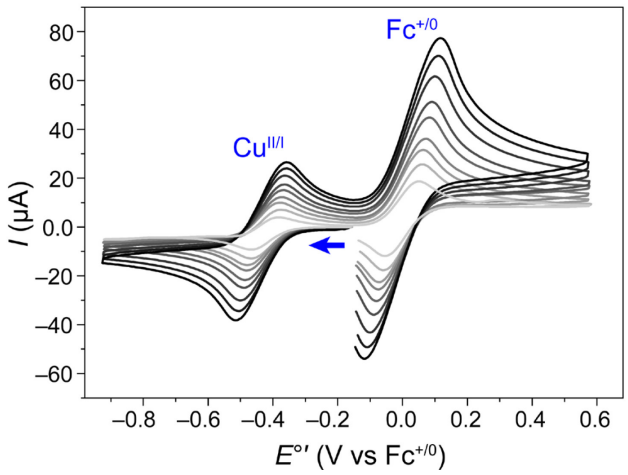

Figure 3. Cyclic voltammograms (CVs) of 1 mM $[CuCl(dpa^{SMe})]^+$ in DCM with 100 mM $[NBu_4]PF_6$ as supporting electrolyte were collected in the presence of $Fc^{+/0}$ varying scan rate from ν = 25–500 mV/s (light to dark). All scans were initiated from open circuit potential, indicated by the arrow.

electrochemistry, which tends to involve large peak-to-peak separations as a consequence of the large reorganization energies typically associated with interchange between Cu^{II} and Cu^{I}. The reversibility observed here suggests a low reorganization energy may be associated with electron transfer in these systems. Of additional note is that under these experimental conditions, a second $Cu^{II/I}$ redox event is not observed at any scan rate (Figure S7). This observation indicates that the conformational equilibrium discussed above is faster than electron transfer with the electrode in this system.[24]

Discussion

The stereochemistry of Cu^{II} ions is reported to be a consequence of many interrelated factors including Jahn-Teller distortions, plasticity (*e.g.* Berry pseudorotation), and constraints imposed by the flexibility (or lack thereof) of the ligand field.[21,25–27] In the context of five-coordinate complexes, these factors give rise to structural variation between ideal square pyramidal and trigonal bipyramidal polyhedra with varying degrees of distortion and geometric distributions. Tripodal ligand frameworks such as tris(2-pyridylmethyl)amine (tpa) and tris(2-aminoethyl)amine (tren) tend to adopt trigonal bipyramidal geometries when bound to Cu^{II}.[16,28–30] Notably, derivatives of these motifs have been shown to preferentially adopt square pyramidal geometries as the steric bulk of the ligands are increased.[31] The examples discussed above represent complexes which are discretely trigonal bipyramidal or square pyramidal, with no reports of conformational dynamicity between the two. There are some reports of Cu^{II} complexes in equilibrium between square pyramidal and trigonal bipyramidal coordination geometries. However, these reports rely on indirect measurements of the dynamics at play,[32,33] where, using modified tren ligands, interconversion from trigonal bipyramidal to square pyramidal geometry was inferred from acid-mediated decomplexation kinetics measurements.

In our system, we are able to observe both geometric isomers crystallographically and via solution and solid-state EPR spectroscopy, allowing for direct observation of conformational dynamics in a Cu^{II} complex. Despite their unique spectroscopic features, the bond metrics for the inner coordination sphere of both geometries are remarkably similar. They have relatively small differences in the bond distances for all bonds except for a ~0.2 Å contraction of the Cu–S distance on going from square pyramidal to trigonal bipyramidal. As highlighted in Figure 1d, the major structural difference arises from the bond angles, which can be attributed to rotation of one picolyl arm, in line with a Berry mechanism.[34]

We have previously reported on the analogous series of dpa^{OMe} complexes, where -OMe replaces the -SMe substituent discussed in this work. We found that these systems exhibit conformationally dynamic Cu^{I} complexes but rigidly square pyramidal Cu^{II} complexes.[10] This rigidity was suggested by XRD, as well as EPR and UV-vis absorption spectroscopies. To date, we have not observed a trigonal bipyramidal geometry for $[CuCl(dpa^{OMe})]^+$ and all attempts to optimize the geometry of this complex by DFT starting from a trigonal bipyramid collapse into the corresponding square pyramidal species. Unlike in the case of the non-dynamic series of complexes in which systematic steric modifications result in changes to the observed coordination geometry,[16,31] we do not believe such steric factors are at play in the structural dynamics of $[CuCl(dpa^{SMe})]^+$ or in the structural rigidity of $[CuCl(dpa^{OMe})]^+$. Instead, we propose that the increased covalency of the Cu–S bond relative to Cu–O plays a significant role in stabilizing the trigonal bipyramidal isomer of the $[CuCl(dpa^{SMe})]^+$ and precluding its formation in $[CuCl(dpa^{OMe})]^+$. The ~0.2 Å contraction of the Cu–S to 2.4013(6) Å in the trigonal bipyramidal structure suggests that the ability of this ligand to stabilize both coordination geometries – and in particular the trigonal bipyramid – is an essential factor in enabling the observed structural dynamics.

Of particular interest is the reversible electrochemistry of $[CuCl(dpa^{SMe})]^{+/0}$, which suggests comparatively minor structural reorganization associated with the $Cu^{II/I}$ couple in these systems. Structural dynamics in molecular copper complexes have been implicated in their electron transfer kinetics.[1,35–39] Moreover, biological electron transfer is often mediated by copper proteins in which the coordination environment surrounding the metal centre is precisely controlled. As such, $[CuCl(dpa^{SMe})]^{+/0}$ represents an intriguing motif for the design of biomimetic redox mediators.

Experimental

General Considerations

Unless otherwise noted, all manipulations were carried out under anaerobic conditions using standard Schlenk line and glovebox techniques. A glovebox in which oxygen is excluded but water is present was employed for all manipulations except electrochemical experiments, which were performed in a dry (water-free) glovebox.

Materials

Acetonitrile (MeCN), methanol (MeOH), pentane, and di-chloromethane (DCM), obtained from Fisher Scientific were purified further using a Jorg C. Meyer Solvent Purification System in which hydrocarbon and ethereal solvents were sparged with nitrogen before being deoxygenated and dried by passage through Q5 and

activated alumina columns, respectively. Halogenated solvents were sparged with nitrogen and passed through two activated alumina columns. Toluene was obtained from Fisher Scientific. Water was obtained from a Milli-Q purification system at 18 MΩ-cm resistivity. $CuCl_2(H_2O)_2$ was obtained from Fisher Scientific, NH_4PF_6 from Alfa Aesar, and all deuterated solvents were from Cambridge Isotope Laboratory. CuCl, obtained from Mallinckrodt was stirred in acetic acid (AcOH) and subsequently washed with ethanol and Et_2O before use (300 mL AcOH per 10 g CuCl). Ferrocene (Fc^0) was purified by recrystallization from hexanes and $[Bu_4N]PF_6$ (Oakwood Chemicals) was recrystallized thrice from ethanol and dried under vacuum. The dpa^{SMe} ligand has been previously reported,[14] but was synthesized here via an alternative strategy in which the pure product could be isolated as a crystalline solid without the need for further chromatographic steps (Scheme S1).

Physical Methods and Instrumentation

^1H and ^{13}C-NMR data were collected on a Bruker spectrometer operating at 600 MHz at ambient temperatures. Chemical shifts are referenced to the residual solvent peaks of CD_2Cl_2 (δ 5.32 ppm for ^1H and δ 53.84 for ^{13}C).[40] Perpendicular mode X-band EPR spectra were collected using a Bruker EMX spectrometer equipped with a ER041XG microwave bridge using the following spectrometer settings: attenuation = 25 dB, micro-wave power = 0.63 mW, frequency = 9.42 GHz, modulation amplitude = 4.0 G, gain = 30 dB, conversion time = 16.00 ms, time constant = 5.12 ms, sweep width = 2000 G and resolution = 3750 points. Samples for solid-state EPR at room temperature were prepared as 50:50 v/v mixtures of Cu^{II} analyte with $[NBu_4]PF_6$. Variable-temperature solution-phase EPR spectra were collected using a MercuryiTC temperature controller from Oxford Instruments and using liquid He as coolant. EPR spectra were modelled using EasySpin/Matlab.[41] High-resolution mass spectra (HRMS) were obtained on a Waters Synapt G2-Si ESI instrument at the UIUC School of Chemical Sciences Mass Spectrometry Laboratory. CHN elemental analyses were collected on an Exeter Analytical CE 440 instrument in the UIUC School of Chemical Sciences Microanalysis Laboratory.

Electrochemistry

Electrochemical experiments were performed on a Pine Wavedriver 10 potentiostat using a 3.0 mm glassy carbon working electrode, a Pt wire auxiliary electrode, and Ag wire pseudo-reference electrode. Data acquisition was carried out at ambient temperature (20−24 °C) in a nitrogen-filled glovebox for solution samples containing 1.0 mM of analyte and 100 mM of $[Bu_4N]PF_6$ supporting electrolyte dissolved in dry, degassed DCM. All potentials were referenced to $Fc^{+/0}$ by adding Fc^0 as an internal standard at the end of each experimental run.[42] All scans were initiated from open circuit potential (OCP).

Single Crystal XRD

XRD data were collected on a Bruker D8 Venture kappa diffractometer equipped with a Photon II CPAD detector. An Iμs microfocus source provided the Mo Kα radiation (λ = 0.71073 Å) that was monochromated with multilayer mirrors.[43] The collection, cell refinement, and integration of intensity data were carried out with the APEX3 software. Multi-scan absorption corrections were performed numerically with SADABS. The initial structure solution was solved with either intrinsic phasing methods SHELXT[44] or direct methods and refined with the full-matrix least-squares SHELXL[45] program within the OLEX2 GUI.[46] Detailed data collection parameters and refinement methods are included in Tables S2−S4 of the Supporting Information (SI).

Computational Chemistry

Density functional theory (DFT) calculations were undertaken using Orca software (version 4).[47] All geometries were optimized without constraints and confirmed as local minima by accompanying frequency calculations using the three-parameter hybrid functional for exchange by Becke and the Lee-Yang-Parr correlation functional (B3LYP)[48,49] using a triple-ζ basis set (def2-TZVP)[50] and chain-of-sphere approximation (RIJCOSX).[51] Isosurfaces were obtained via couple-perturbed self-consistent field (CP-SCF) calculations accounting for spin-orbit coupling at Cu.[52–54] DFT optimized coordinates are provided in Tables S6 and S7.

Preparation of Complexes

CuCl(dpa^{SMe}). CuCl (0.065 g, 0.66 mmol) was added to a Schlenk flask equipped with a stir bar, placed under N_2, and dissolved in degassed MeCN (6 mL, ~0.1 M). dpa^{SMe} (0.192 g, 0.60 mmol) was dissolved in degassed MeCN (6 mL, ~0.1 M) in a separate vial and added to the stirred solution of CuCl dropwise. The reaction was heated to reflux for 15 min before cooling to room temperature, at which point it was left to stir overnight in a wet glovebox. The reaction was then filtered over celite, the celite rinsed with MeCN (25 mL), and the solution concentrated under reduced pressure. The resulting pale-yellow solid was dissolved in minimal DCM and pentane was added to induce precipitation. The cloudy solution was allowed to sit for 2 h, during which yellow crystals of the product began to form. These crystals were rinsed with pentane and allowed to dry under vacuum to afford the product as yellow crystals (0.240 g, 96%). Golden crystals suitable for XRD could be grown at room temperature, overnight, by vapour diffusion of pentane into a solution of complex in DCM. ^1H NMR (CD_2Cl_2, 600 MHz): 9.04 (s, br, 2H), 7.71 (s, br, 2H), 7.48 (s, br, 1H), 7.36-7.16 (m, 5 H), 7.14 (t, J = 7.37 Hz, 2H), 4.29 (s, 4H), 2.58 (s, 3H). HRMS: ESI Positive ion mode m/z [M^+] calcd.: 419.0284, found: 419.0277. Anal. calcd. for: $C_{19}H_{19}ClCuN_3S$•0.5 CH_2Cl_2, found: C, 49.94 (50.60); H, 4.32(4.35); N, 8.91(9.08).

[CuCl(dpa^{SMe})]PF_6. dpa^{SMe} (0.100 g, 0.31 mmol) was dissolved in minimal MeOH (2 mL) in a vial equipped with a stir bar under air. In a separate vial, $CuCl_2(H_2O)_2$ (0.058 g, 0.34 mmol) was dissolved in water (1 mL) and the resulting solution added dropwise to the stirring dpa^{SMe} solution. After 15 min, NH_4PF_6 (0.203 g, 1.24 mmol) was added and the resulting precipitate was allowed to stir for an additional 15 min before filtering. The precipitate was rinsed with water and allowed to dry to afford the product as a cyan solid (0.127 g, 72%). Crystals suitable for XRD could be grown at –20 °C by vapour diffusion of pentane into a solution of the complex in DCM or by layer diffusion of a methanolic solution of complex into water. HRMS: ESI Positive ion mode m/z [M^+] calcd.: 419.0287, found: 419.0284. Anal. calcd. for: $C_{19}H_{19}CuClN_3SPF_6$, found: C, 40.36 (40.51); H, 3.39 (3.30); N, 7.43 (7.43).

Conclusions

The conformational dynamics of Cu^{II} complexes containing a dpa^{SMe} ligand were explored via solid-state and solution-phase measurements**.** Solid-state measurements revealed that $[CuCl(dpa^{SMe})]^{+}$ exhibits both discrete trigonal bipyramidal and square pyramidal geometries in the solid state as assessed by single crystal XRD and in bulk samples via powder EPR spectroscopy. Solution-phase EPR spectra indicate that solutions of the Cu^{II} complex are best described as mixtures of the two stereoisomers, where the trigonal bipyramidal coordination geometry predominates at room temperature and the square pyramidal coordination geometry predominates at low temperature. These dynamics are enabled by the relative flexibility of the ligand backbone and the ability of Cu–S covalency to stabilize the trigonal bipyramidal conformer. The reversible electrochemistry of these complexes suggest that $[CuCl(dpa^{SMe})]^{+/0}$ is capable of facilitating rapid and reversible electron transfer.

Acknowledgements

The authors gratefully acknowledge Dr. Toby Woods for assistance with variable-temperature EPR spectroscopy and Dr. Khadanand KC for helpful discussions. This work was supported by the U. S. Department of Energy, Office of Science, Basic Energy Sciences under Award # DE-SC0022846.

Notes and references

1 D. B. Rorabacher, *Chem. Rev.*, 2004, **104**, 651–697.
2 R. R. Conry, in *Encyclopedia of Inorganic Chemistry*, eds. R. B. King, R. H. Crabtree, C. M. Lukehart, D. A. Atwood and R. A. Scott, John Wiley & Sons, Ltd, Chichester, UK, 2006, p. ia052.
3 E. I. Solomon, R. K. Szilagyi, S. DeBeer George and L. Basumallick, *Chem. Rev.*, 2004, **104**, 419–458.
4 E. I. Solomon and R. G. Hadt, *Coord. Chem. Rev.*, 2011, **255**, 774–789.
5 B. L. Vallee and R. J. Williams, *Proc. Natl. Acad. Sci.*, 1968, **59**, 498–505.
6 B. G. Malmström, *Biol. Met.*, 1990, **3**, 64–66.
7 P. Comba, *Coord. Chem. Rev.*, 2000, **200–202**, 217–245.
8 J. Stanek, A. Hoffmann and S. Herres-Pawlis, *Coord. Chem. Rev.*, 2018, **365**, 103–121.
9 P. J. Griffin, B. J. Charette, J. H. Burke, J. Vura-Weis, R. D. Schaller, D. J. Gosztola and L. Olshansky, *J. Am. Chem. Soc.*, 2022, **144**, 12116–12126.
10 B. J. Charette, P. J. Griffin, C. M. Zimmerman and L. Olshansky, *Dalton Trans.*, 2022, **51**, 6212–6219.
11 R. G. Pearson, *J. Am. Chem. Soc.*, 1963, **85**, 3533–3539.
12 L. Yang, D. R. Powell and R. P. Houser, *Dalton Trans.*, 2007, 955–964.
13 H. R. Lucas, L. Li, A. A. N. Sarjeant, M. A. Vance, E. I. Solomon and K. D. Karlin, *J. Am. Chem. Soc.*, 2009, **131**, 3230–3245.
14 Y. Lee, D.-H. Lee, G. Y. Park, H. R. Lucas, A. A. Narducci Sarjeant, M. T. Kieber-Emmons, M. A. Vance, A. E. Milligan, E. I. Solomon and K. D. Karlin, *Inorg. Chem.*, 2010, **49**, 8873–8885.
15 A. W. Addison, T. N. Rao, J. Reedijk, J. van Rijn and G. C. Verschoor, *J. Chem. Soc. Dalton Trans.*, 1984, 1349–1356.
16 K. D. Karlin, J. C. Hayes, S. Juen, J. P. Hutchinson and J. Zubieta, *Inorg. Chem.*, 1982, **21**, 4106–4108.
17 S. Fox, A. Nanthakumar, M. Wikström, K. D. Karlin and N. J. Blackburn, *J. Am. Chem. Soc.*, 1996, **118**, 24–34.
18 D.-H. Lee, L. Q. Hatcher, M. A. Vance, R. Sarangi, A. E. Milligan, A. A. Narducci Sarjeant, C. D. Incarvito, A. L. Rheingold, K. O. Hodgson, B. Hedman, E. I. Solomon and K. D. Karlin, *Inorg. Chem.*, 2007, **46**, 6056–6068.
19 B. J. Hathaway and D. E. Billing, *Coord. Chem. Rev.*, 1970, **5**, 143–207.
20 A. M. Q. Vande Linde, B. C. Westerby, L. A. Ochrymowycz and D. B. Rorabacher, *Inorg. Chem.*, 1993, **32**, 251–257.
21 B. J. Hathaway, *J Chem Soc Dalton Trans*, 1972, 1196–1199.
22 Z.-W. Mao, G. Liehr and R. van Eldik, *J. Chem. Soc. Dalton Trans.*, 2001, 1593–1600.
23 S. Stoll, in *Encyclopedia of Biophysics*, ed. G. C. K. Roberts, Springer Berlin Heidelberg, Berlin, Heidelberg, 2013, pp. 2316–2316.
24 N. M. Villeneuve, R. R. Schroeder, L. A. Ochrymowycz and D. B. Rorabacher, *Inorg. Chem.*, 1997, **36**, 4475–4483.
25 B. J. Hathaway and P. G. Hodgson, *J. Inorg. Nucl. Chem.*, 1973, **35**, 4071–4081.
26 B. J. Hathaway, in *Complex Chemistry*, Springer Berlin Heidelberg, Berlin, Heidelberg, 1984, vol. 57, pp. 55–118.
27 J. Gažo, L. Bersuker, J. Garaj, M. Kabešová, J. Kohout, H. Langfelderová, M. Melník, M. Serátor and F. Valach, *Coord. Chem. Rev.*, 1976, **19**, 253–297.
28 H.-K. Fun, B.-C. Yip, Z. Lu, C.-Y. Duan, Y.-B. Tian and X.-Z. You, *Transit. Met. Chem.*, 1996, **21**, 193–196.
29 A. M. Dittler-Klingemann and F. E. Hahn, *Inorg. Chem.*, 1996, **35**, 1996–1999.
30 A. G. Blackman, *Polyhedron*, 2005, **24**, 1–39.
31 N. Wei, N. N. Murthy and K. D. Karlin, *Inorg. Chem.*, 1994, **33**, 6093–6100.
32 A. G. Algarra, M. G. Basallote, C. E. Castillo, M. P. Clares, A. Ferrer, E. García-España, J. M. Llinares, M. A. Máñez and C. Soriano, *Inorg. Chem.*, 2009, **48**, 902–914.
33 C. E. Castillo, A. G. Algarra, M. Á. Máñez, C. Duboc and M. G. Basallote, *Eur. J. Inorg. Chem.*, 2012, **2012**, 2514–2526.
34 R. S. Berry, *J. Chem. Phys.*, 1960, **32**, 933–938.
35 K. Krylova, C. P. Kulatilleke, M. J. Heeg, C. A. Salhi, L. A. Ochrymowycz and D. B. Rorabacher, *Inorg. Chem.*, 1999, **38**, 4322–4328.
36 G. Chaka, J. L. Sonnenberg, H. B. Schlegel, M. J. Heeg, G. Jaeger, T. J. Nelson, L. A. Ochrymowycz and D. B. Rorabacher, *J. Am. Chem. Soc.*, 2007, **129**, 5217–5227.
37 E. A. Ambundo, M.-V. Deydier, A. J. Grall, N. Aguera-Vega, L. T. Dressel, T. H. Cooper, M. J. Heeg, L. A. Ochrymowycz and D. B. Rorabacher, *Inorg. Chem.*, 1999, **38**, 4233–4242.
38 E. A. Ambundo, L. A. Ochrymowycz and D. B. Rorabacher, *Inorg. Chem.*, 2001, **40**, 5133–5138.
39 E. A. Ambundo, Q. Yu, L. A. Ochrymowycz and D. B. Rorabacher, *Inorg. Chem.*, 2003, **42**, 5267–5273.
40 G. R. Fulmer, A. J. M. Miller, N. H. Sherden, H. E. Gottlieb, A. Nudelman, B. M. Stoltz, J. E. Bercaw and K. I. Goldberg, *Organometallics*, 2010, **29**, 2176–2179.
41 S. Stoll and A. Schweiger, *J. Magn. Reson.*, 2006, **178**, 42–55.
42 N. G. Connelly and W. E. Geiger, *Chem. Rev.*, 1996, **96**, 877–910.
43 L. Krause, R. Herbst-Irmer, G. M. Sheldrick and D. Stalke, *J. Appl. Crystallogr.*, 2015, **48**, 3–10.
44 G. M. Sheldrick, *Acta Crystallogr. Sect. A*, 2015, **71**, 3–8.
45 G. M. Sheldrick, *Acta Crystallogr. Sect. C*, 2015, **71**, 3–8.

46 O. V. Dolomanov, L. J. Bourhis, R. J. Gildea, J. A. K. Howard and H. Puschmann, *J. Appl. Crystallogr.*, 2009, **42**, 339–341.
47 F. Neese, *WIREs Comput. Mol. Sci.*, 2012, **2**, 73–78.
48 A. D. Becke, *J. Chem. Phys.*, 1993, **98**, 5648–5652.
49 C. Lee, W. Yang and R. G. Parr, *Phys. Rev. B*, 1988, **37**, 785–789.
50 F. Weigend and R. Ahlrichs, *Phys Chem Chem Phys*, 2005, **7**, 3297–3305.
51 F. Neese, F. Wennmohs, A. Hansen and U. Becker, *Chem. Phys.*, 2009, **356**, 98–109.
52 F. Neese, *J. Chem. Phys.*, 2001, **115**, 11080–11096.
53 F. Neese, *J. Chem. Phys.*, 2003, **118**, 3939–3948.
54 F. Neese, *Curr. Opin. Chem. Biol.*, 2003, **7**, 125–135.